Immune checkpoint remodeling across disease progression in multiple myeloma

Zuzana VALUSKOVA[1], Dana CHOLUJOVA[1], Gabor BEKE[2], Milan HUCKO[2], Lubos KLUCAR[2], Gabriela GROFOVA[1], Lubos DRGONA[3], Jana JAKUBIKOVA[1,4,*]

[1]Department of Tumor Immunology, Cancer Research Institute, Biomedical Research Center, Slovak Academy of Sciences, Bratislava, Slovakia; [2]Institute of Molecular Biology, Slovak Academy of Sciences, Bratislava, Slovakia; 3Department of Oncohematology, Comenius University and National Cancer Institute, Bratislava, Slovakia; 4Centre for Advanced Material Application, Slovak Academy of Sciences, Bratislava, Slovakia

*Correspondence: jana.jakubikova@savba.sk

Immune checkpoint dynamics within the bone marrow (BM) critically shape disease evolution and therapeutic responses in multiple myeloma (MM). To delineate immune remodeling in the BM during plasma cell malignancy evolution, we profiled inhibitory (PD-1, CTLA-4, LAG-3, TIM-3, TIGIT, BTLA, and 2B4) and co-stimulatory (ICOS, CD27, DNAM-1, 4-1BB, and OX40) checkpoints across adaptive and select innate compartments in healthy donors (HD, n=25), monoclonal gammopathy of undetermined significance (MGUS, n=17), newly diagnosed MM (NDMM, n=57), and relapsed/relapsed-refractory MM (MM, n=72; on-treatment n=27, off-treatment n=12). Progressive disease featured loss of mature, memory, and activated/proliferating B cell subsets and an NDMM-specific expansion of plasmablasts/plasma cells. B cell maturation was accompanied by broad remodeling of inhibitory receptors (notably reduced PD-1, TIM-3, TIGIT, and 2B4 on mature B cells; decreased CTLA-4 on activated B cells and plasmablasts/plasma cells; and reduced TIM-3, LAG-3, and 2B4 on plasmablasts/plasma cells) alongside selective co-stimulatory changes (OX40 decreased on mature B cells; CD27 loss on activated and plasmablast/plasma compartments; divergent 4-1BB regulation). T cell compartments showed early CD4$^+$ expansion with CD8$^+$ cytotoxic reduction and checkpoint shifts: broad PD-1 downregulation with subset-restricted increases in LAG-3, TIM-3, TIGIT, and BTLA; variable upregulation of CD27, DNAM-1, and ICOS; and consistent 4-1BB loss. NKT and γδ T cell frequencies were stable, but their checkpoints were reconfigured: NKT cells exhibited decreased PD-1 and 4-1BB and increased TIGIT, LAG-3, and DNAM-1, whereas γδ T cells showed reduced CTLA-4, BTLA, and the co-stimulatory receptor OX40. Innate NK cells demonstrated reduced frequency and phenotypic shifts, including decreased TIM-3 and PD-1, loss of 4-1BB and OX40, stage-specific increases in TIGIT and 2B4, and elevated DNAM-1. Checkpoint alterations, such as low TIGIT or CTLA-4 and elevated OX40 expression, were correlated with superior progression-free survival. MM progression entails extensive, stage- and subset-specific remodeling of inhibitory and activating immune checkpoints in the BM, with implications for immunotherapeutic targeting.

Key words: multiple myeloma, immune microenvironment, immune checkpoints, flow cytometry

Multiple myeloma (MM) is a hematologic malignancy driven by the clonal expansion of terminally differentiated plasma cells within the bone marrow (BM), resulting in marrow infiltration, monoclonal protein secretion, end-organ damage (bone lesions, anemia, hypercalcemia, renal dysfunction), and pronounced clinical and biological heterogeneity in disease course and treatment response [1]. MM evolves through premalignant stages, such as monoclonal gammopathy of undetermined significance (MGUS) and smoldering multiple myeloma (SMM), which are defined by progressively higher tumor burden and biomarker abnormalities without overt end-organ damage. Although many individuals with MGUS remain stable, a subset progress to SMM and ultimately symptomatic MM as genetic lesions accumulate and the bone-marrow niche changes [2, 3]. Recurrent genetic alterations in MM (for example, IGH translocations, hyperdiploidy, and segmental copy-number changes) drive clonal evolution, yet mounting evidence indicates that the BM tumor microenvironment critically shapes malignant plasma cell survival, its therapeutic resistance, and disease progression [4–6]. Despite substantial survival gains from novel targeted agents and immunotherapies, including proteasome inhibitors, immunomodulatory drugs, CD38-directed monoclonal antibodies, BCMA-targeted antibody–drug

conjugates, bispecific T-cell engagers, and CAR T-cell therapies, MM remains largely incurable [7], underscoring the need for continued elucidation of disease pathogenesis and the development of strategies capable of producing durable, disease-eradicating remissions.

The BM immune microenvironment undergoes progressive, multi-lineage remodeling from premalignant stages (MGUS, SMM) to active MM, creating an immunosuppressive niche that fosters tumor survival and immune escape [8, 9]. Early and recurrent alterations include dysfunctional dendritic cells with decreased HLA-DR, expansion of myeloid-derived suppressor cells, and shifts in NK- and T-cell compartments that compromise antigen presentation and cytotoxic immunity [10, 11]. High-dimensional approaches, such as mass cytometry (CyTOF), single-cell RNA sequencing, and computational deconvolution, have systematically mapped these changes and shown loss of cytotoxic CD8$^+$ T cells, perturbation of central and effector memory T-helper and cytotoxic subsets, depletion of progenitor/transitional B cells, and an enrichment of monocytic and neutrophil subsets during progression [12–14]. Integrative multi-omics and spatial single-cell atlases further resolve distinct immune subtypes and osteoclast-driven immunosuppressive programs, linking microenvironmental states to tumor subclonal architecture, prognosis, and therapy response [5, 15–17]. Longitudinal profiling before and during therapy has identified immune phenotypes associated with clinical benefit (e.g., preserved cytotoxic and mature NK signatures) versus those linked to resistance (myeloid/monocytic expansion, antigen-presentation defects) [13]. Together, these convergent findings demonstrate that dynamic immune dysregulation is a critical driver of MM pathogenesis and therapeutic outcome and nominate tractable immunomodulatory targets for interceptive and combination strategies.

Distinct alterations in immune-checkpoint expression characterize the BM tumor microenvironment in MM across the continuum from precursor states to active disease. Parallel CyTOF proteomic analyses in our cohort and in an independent study demonstrate checkpoint remodeling across innate and adaptive compartments, including NK cells, monocytes, and dendritic cells, with phenotypes that associate with antigen-presentation defects and exhaustion programs [12, 18]. Using single-cell transcriptomics, CyTOF, single-cell proteomics, and integrated bulk and metabolic profiling, studies have detected early and progressive upregulation of inhibitory receptors, including PD-1, TIM-3, LAG-3, and TIGIT on T cells, frequently as co-expressed modules characteristic of clonally expanded, dysfunctional T-cell populations [10, 12, 19]. Machine-learning integration of multi-omics datasets has distilled reproducible checkpoint signatures that correlate with prognosis and treatment response, supporting their utility as predictive biomarkers [17, 20]. Ongoing clinical studies targeting TIGIT, TIM-3, LAG-3, and other inhibitory receptors are already informed

by these molecular and cellular insights. Collectively, these high-dimensional investigations nominate specific checkpoint pathways as rational targets for precision, biomarker-driven immunotherapeutic strategies in MM.

In this study, we conducted a comprehensive profiling of key inhibitory (PD-1, CTLA-4, LAG-3, TIM-3, TIGIT, BTLA, and 2B4) and co-stimulatory (ICOS, CD27, DNAM-1, 4-1BB, and OX40) immune checkpoint molecules across adaptive and selected innate immune populations within the BM microenvironment. BM samples were analyzed from patients with MGUS, newly diagnosed MM (NDMM), relapsed/relapsed-refractory MM (MM), and healthy donors (HD). Using two complementary antibody panels and high-parameter flow cytometry, we systematically assessed checkpoint expression and immune subset composition across major B cell, T cell, and NK cell compartments. This analysis provides a high-resolution, subset-specific characterization of immune checkpoint remodeling across disease progression and treatment conditions, offering an in-depth overview of immune subset composition and checkpoint expression in MM that advances our understanding of immune dysregulation, highlights potential targets for immunotherapeutic intervention, and demonstrates their relevance as prognostic biomarkers in MM.

Patients and methods

Patient cohort and clinical specimen collection. A total of 171 BM specimens were included in this study: 17 samples from individuals with MGUS; 57 samples from patients with NDMM; 72 samples from relapsed or relapsed/refractory multiple myeloma (MM), with MM cases further stratified as on treatment (MMinTx; n=27) or off treatment (MMnoTx; n=12); and 25 samples of non-malignant (healthy) BM obtained from femoral heads during elective hip arthroplasty. Patients with MGUS and MM were consecutively recruited from clinical hospital diagnostic and treatment services, and BM aspirates were obtained from the posterior iliac crest during routine diagnostic or staging procedures. Healthy control BM specimens were aseptically harvested from femoral heads resected during hip replacement surgeries and confirmed to be free of hematologic disease. Demographic and key clinical characteristics of the cohort (age, sex, disease stage, prior therapy, biomarkers, and relevant laboratory parameters) are summarized in Supplementary Table S1. All participants provided written informed consent prior to inclusion. The study protocol was conducted in accordance with the Declaration of Helsinki and was approved by the Institutional Human Ethics Committee of the Biomedical Research Center in Bratislava, Slovakia, under reference number Myelom 001. Immediately after collection, specimens were assigned a unique study identifier, de-identified, and handled according to institutional standard operating procedures to minimize pre-analytical variability. Consent forms and clinical data linkage were managed to preserve

participant confidentiality; only coded identifiers were used for laboratory analyses and data reporting.

Specimen stabilization, storage, and pre-analytical processing. BM aspirates designated for cytometric analysis were immediately stabilized by the addition of Streck Cell Preservative (Streck, La Vista, NE, USA) at a 1:1 volume ratio (sample:preservative) to preserve leukocyte morphology and antigenic integrity. Following stabilization, specimens were stored at 4 °C and processed within seven days of collection. Prior to immunostaining and data acquisition, samples were equilibrated to ambient laboratory temperature (approximately 20–25 °C) and gently homogenized by 25 inversions, per the manufacturer's instructions. After equilibration and mixing, samples were processed without undue delay.

High-dimensional multiparametric flow cytometric immunophenotyping. All antibodies, antibody clones, conjugated fluorochromes, manufacturers, and final working dilutions are listed in Supplementary Table S2. Samples designated for the intracellular workflow (LST-1) or the surface workflow (LST-2) were processed according to the protocol specifics described below. For each staining condition, 80 µl of a thoroughly mixed BM cell suspension was transferred to a tube, and the appropriate antibody cocktail, prepared immediately before use, was added directly to the aliquot. All incubations and light-sensitive manipulations were carried out protected from light.

The LST-1 workflow combined surface staining with subsequent intracellular detection of cytoplasmic immunoglobulin light chains. Surface antigens were stained by adding the LST-1 surface antibody cocktail to 80 µl aliquots and incubating for 30 min at room temperature (RT) in the dark. After surface labeling, samples were washed twice with PBS/0.5% BSA (600×g, 6 min, RT for each wash) to remove unbound antibody. Cells were then fixed and permeabilized by incubating in 100 µl BD Cytofix/Cytoperm Fixation/ Permeabilization Solution (BD Biosciences, Franklin Lakes, NJ, USA) for 15 min at RT in the dark, following the manufacturer's protocol. Following fixation/permeabilization, cells were washed once in 1× BD Perm/Wash buffer (prepared from 10× BD Perm/Wash Buffer in sterile water) and pelleted by centrifugation at 600×g for 6 min at RT. The pellet was resuspended in 100 µl Perm/Wash buffer and incubated with intracellular antibodies directed against cytoplasmic κ and λ light chains for 30 minutes at RT in the dark. After intracellular labeling, samples were washed with PBS/0.5% BSA (600×g, 6 min, RT) and resuspended in 200 µl PBS/0.5% BSA for acquisition.

For the LST-2 surface immunophenotyping workflow, after gentle mixing by pipetting, samples were incubated with the LST-2 antibody panel for 30 min at RT in the dark to allow binding of surface antibodies. Red blood cells were lysed by adding 2 ml of BD FACS™ Lysing Solution (BD Biosciences, San Jose, CA, USA) and incubating for 10 min at RT in the dark, following the manufacturer's instructions. Lysed samples were then washed twice with PBS/0.5% BSA;

each wash consisted of centrifugation at 600×g for 6 min at RT and careful aspiration of the supernatant. After the final wash, cell pellets were resuspended in 200 µl PBS/0.5% BSA, and samples were analyzed on a flow cytometer.

Data acquisition and analysis. Acquisition for both LST-1 and LST-2 panels was performed on a BD FACSAria™ flow cytometer equipped with a UV laser (Becton Dickinson, Mountain View, CA, USA). For each patient sample, a minimum of $5.0×10^5$ events was recorded to ensure robust population representation and downstream statistical power. Instrument performance and daily stability were confirmed using manufacturer-recommended quality control beads; compensation was performed using single-color controls, unstained controls, and fluorescence-minus-one (FMO) controls to define gating boundaries for dim populations. Acquired data were analyzed using De Novo FCS Express software; detailed gating strategies of representative plots are provided in the Supplementary Figure S1.

Gating strategy and cytometric data processing. Flow cytometric data were inspected and processed using a standardized, reproducible workflow. Raw FCS files were inspected for acquisition anomalies; all downstream gating and metric extraction were performed in De Novo FCS Express 7 (De Novo Software, CA, USA). During initial preprocessing, doublets and debris were excluded by sequential gating on forward scatter height versus width (FSC-H vs. FSC-W and SSC-H vs. SSC-W) and on forward versus side scatter (FSC vs. SSC). Leukocyte populations were then delineated using a hierarchical strategy: a CD45 versus SSC gate was used to select leukocytes, and singlet CD45⁺ events were carried forward for lineage gating.

Within the lymphoid compartment, B cells were defined as CD19⁺CD3⁻ events; helper T cells as CD3⁺CD4⁺ events; cytotoxic T cells as CD3⁺CD8⁺ events; and NK cells as CD3⁻ CD56⁺ events. Malignant plasma cells were identified by a combination of characteristic features, including CD45^low and high CD38 expression within the CD19⁻CD3⁻ population; the gating hierarchy and representative gates are shown in Supplementary Figure S1. For all antigen measurements, positivity thresholds were defined by FMO controls; percent-positive values and median fluorescence intensities (MFI) were reported relative to these empirically derived gates.

Expression of immune checkpoint molecules was quantified on each gated subset. Monoclonal antibodies targeting PD-1, CTLA-4, LAG-3, BTLA, TIM-3, TIGIT, ICOS, OX40, 2B4, DNAM-1, CD27, and 4-1BB were evaluated as percentages of positive cells and as MFI within each defined population. Prior to statistical analysis, all fluorescence channels were inspected for spillover and signal stability; a biexponential/logicle transformation (as implemented in FCS Express) was applied to properly display low- and high-intensity signals and to avoid compression of negative or near-zero values. For exploratory high-dimensional analyses, compensated and transformed data were exported for unsupervised clustering and for dimensionality reduction; Uniform

Manifold Approximation and Projection (UMAP) was used for visualization.

Statistical analysis. All statistical analyses were performed using GraphPad Prism (GraphPad Software), and complementary analyses were carried out in R (version and packages recorded in the project log where applicable). Descriptive statistics are reported as median and interquartile range (IQR) for continuous variables, and as percentages for categorical variables. Group-wise comparisons involving more than two independent groups were tested using the nonparametric Kruskal-Wallis test; when the Kruskal-Wallis test indicated a significant overall effect, pairwise post hoc comparisons were performed using Dunn's correction for multiple comparisons. For survival analyses, progression-free survival (PFS) was estimated using the Kaplan-Meier method, and differences between groups were assessed with the log-rank test. Univariate Cox proportional hazards models were used to identify candidate risk factors for disease progression. p-values (*p<0.05, **p<0.01, ***p<0.001) are shown in graphs and figure legends.

Results

Comprehensive mapping of inhibitory and co-stimulatory immune checkpoints in the BM microenvironment across MM stages using multiparameter flow cytometry. To characterize the dynamics of the BM microenvironment in MM, we systematically profiled key inhibitory (PD-1, CTLA-4, LAG-3, TIM-3, TIGIT, BTLA, 2B4) and co-stimulatory/activation (ICOS, CD27, DNAM-1, 4-1BB, OX40) immune checkpoint molecules across adaptive and selected innate immune compartments within the BM. The study cohort included patients with MGUS (n=17), NDMM (n=57), and relapsed or relapsed/refractory MM (MM; n=72), with MM cases further stratified as on treatment (MMinTx; n=27) or off treatment (MMnoTx; n=12). BM samples from healthy donors served as controls (HD; n=25). Cohort characteristics are summarized in Supplementary Table S1. BM mononuclear/leukocyte fractions (after red blood cell lysis) were stained using two complementary antibody panels (LST1 and LST2; full reagent lists in Supplementary Table S2) and analyzed by multiparameter flow cytometry (Figure 1A). Immune populations interrogated included B cell states (mature/naïve to memory B, activated/proliferating B cells, plasmablasts/plasma cells), T-cell subsets (CD4+ helper, CD8+ cytotoxic, double-negative CD3+CD4−CD8−, double-positive CD3+CD4+CD8+); as well as NKT and γδ T cells, and NK cells from the innate compartment, which were also visualized by UMAP projection (Figure 1B; gating strategy shown in Supplementary Figure S1). We quantified subset frequencies and checkpoint expression to enable high-resolution, subset-specific comparisons of inhibitory and co-stimulatory landscapes across disease stage and treatment status. This high-dimensional flow cytometry approach produced a comprehensive

map of immune-checkpoint expression in the BM, facilitating direct comparison between MGUS, NDMM, MM, and HD.Dynamic regulation of B cell subsets and immune-checkpoint expression across MM stages. B cell populations were identified by gating on CD3−CD19+ lymphocytes. Within the CD19+ compartment, CD19+CD38low cells were classified as mature naïve to memory B cells, and CD19+CD38+ cells as activated/proliferating B cells (including germinal center-like B cells). In contrast, CD19−CD45lowCD38++ cells represented plasmablasts/plasma cells (Figure 2A). Analysis of population distributions revealed a pronounced decline in the frequency of mature naïve to memory B cells across all five MM stages. Activated/proliferating B cells were also decreased in frequency in the NDMM, MM, and MMinTx cohorts. In contrast, the NDMM cohort exhibited an expansion of the plasmablast/plasma cell compartment (Supplementary Figure S2A). A heatmap depicting the relative median expression of inhibitory and stimulatory immune-checkpoint molecules across individual patients and clinical groups (HD and the five MM stages) illustrates subset-specific checkpoint modulation within the CD19+CD38low (mature naïve/memory), CD19+CD38+ (activated/proliferating), and CD19−CD45lowCD38++ (plasmablast/plasma cell) compartments, collectively reflecting a coordinated remodeling of the B-cell checkpoint landscape during MM progression (Figure 2B).

We next examined immune-checkpoint expression within each B-cell subset compared to HD. Among mature naïve to memory B cells, PD-1 expression was reduced in MGUS, NDMM, and MM, and the inhibitory receptors TIGIT, 2B4, and TIM-3 were downregulated in NDMM (TIGIT downregulation was also observed in MGUS). No consistent alterations were detected for CTLA-4, BTLA, or LAG-3 in this B-cell subset. Activated/proliferating B cells were notable for reduced CTLA-4 expression in the MGUS, NDMM, MM, and MMinTx groups; other inhibitory receptors (BTLA, PD-1, TIM-3, TIGIT, 2B4, LAG-3) did not show consistent changes in these cells. Within the plasmablast/plasma cell population, CTLA-4 was downregulated across all five MM stages. TIM-3 expression was decreased in MGUS and NDMM, while LAG-3 and 2B4 were decreased specifically in NDMM. BTLA, PD-1, and TIGIT levels were not significantly altered in the plasmablast/plasma cell compartment (Figure 2C).

Evaluation of co-stimulatory molecules revealed stage- and subset-specific modulation. In the mature naïve to memory B-cell compartment, 4-1BB and OX40 were downregulated in NDMM. In activated/proliferating B cells, 4-1BB was increased in the MMinTx group, and CD27 was decreased in the MM and MMnoTx groups; DNAM-1 and ICOS showed no systematic changes. In plasmablasts/plasma cells, 4-1BB was upregulated in the MM and MMinTx cohorts, whereas CD27 expression was reduced in the NDMM, MM, and MMnoTx groups; ICOS, OX40, and DNAM-1 were unchanged (Figure 2C). Across disease progression, there is a coordinated remodeling of the B-cell compartment charac-
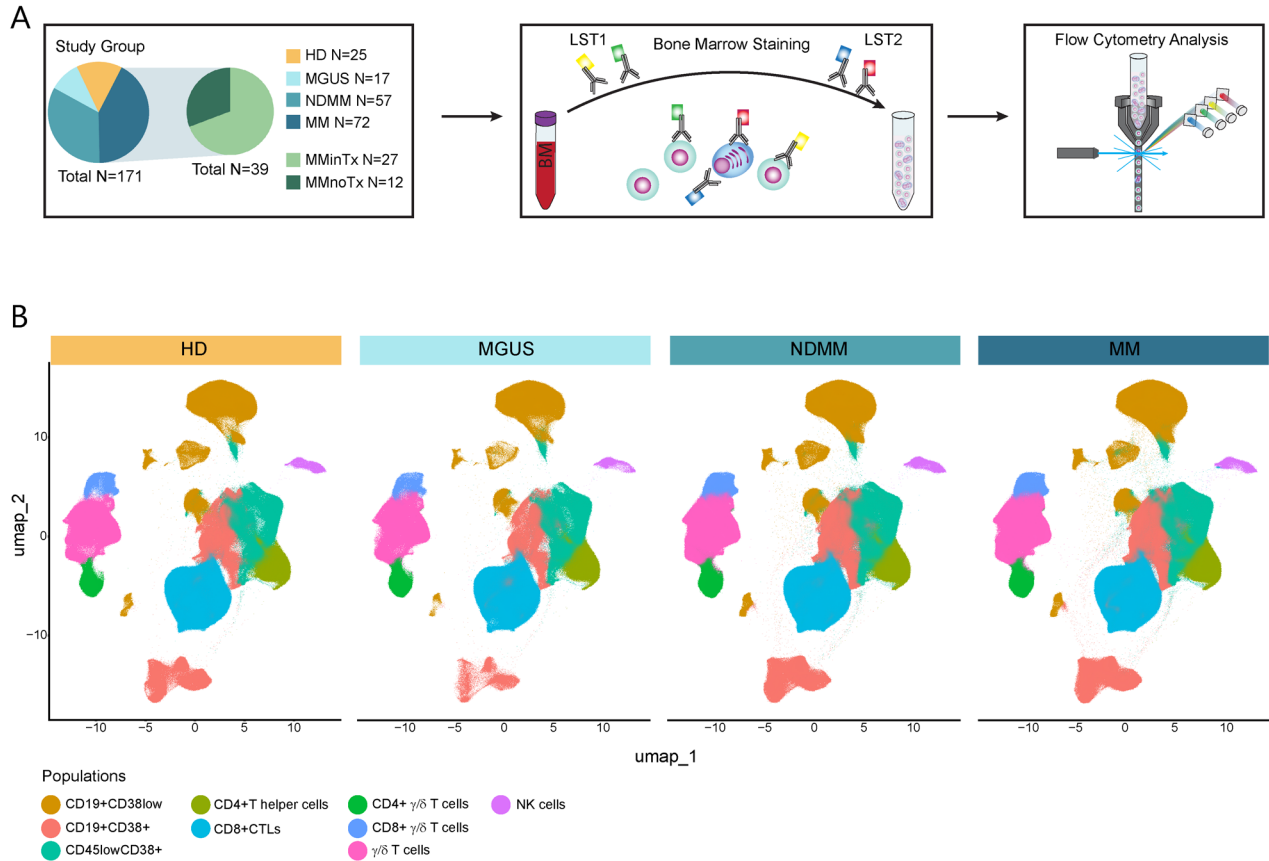
Figure 1. Study design and analytical workflow. (A) Overview of patient cohorts and sample sizes: MGUS (n=17), newly diagnosed MM (NDMM; n=57), relapsed/relapsed-refractory MM (MM; n=72), MM on therapy (MMinTx; n=27), MM off therapy (MMnoTx; n=12), and healthy donor bone marrow (HD; n=25). Experimental workflow: Bone marrow aspirates were processed to obtain mononuclear/leukocyte fractions (via red blood cell lysis), stained with two complementary antibody panels (LST1 and LST2), and analyzed on a multiparameter flow cytometer. (B) UMAP projection illustrating B cell states (mature/naïve to memory B cells, activated/proliferating B cells, plasmablasts/plasma cells), T cell subsets (CD4+ helper and CD8+ cytotoxic), as well as γδ T cells (CD8+ γδ T and CD4+ γδ T) cells and NK cells, in a cohort of HD, MGUS, NDMM, and MM.

terized by depletion of mature and activated B-cell subsets, expansion of plasmablasts/plasma cells in NDMM, and stage-specific dysregulation of inhibitory and stimulatory immune-checkpoint molecules.

Distinct immune-checkpoint profiles in T cell subsets across MM stages. Adaptive T cell subsets were identified by gating on CD3+ lymphocytes, followed by sequential gating into CD4+ T helper cells and CD8+ cytotoxic T lymphocytes (CTLs). CD3+CD4-CD8- (double-negative, CD3+DN T cells) and CD3+CD4+CD8+ (double-positive, CD3+DP T cells) populations were defined as described by the gating strategy (Figure 3A). Relative frequencies compared with HD revealed a selective expansion of CD4+ T helper cells in MGUS and NDMM, whereas CD8+ CTLs were reduced only in MGUS; DN and DP frequencies were not substantially altered in any MM cohort (Supplementary Figure S2B).

A heatmap of the relative median expression of immune-checkpoint molecules across individual patients and clinical groups (HD and five MM stages) demonstrated subset-specific checkpoint remodeling within helper T cells, CTLs, CD3+DN, and CD3+DP T cell populations (Figure 3B). In CD4+ helper T cells, inhibitory receptors showed a differential pattern: BTLA was increased in the combined MM cohort and in the MMnoTx subgroup, and LAG-3 was elevated in MMnoTx; conversely, PD-1 expression was decreased in MGUS, NDMM, MM, and MMinTx. No consistent differences *versus* HD were observed for CTLA-4, TIGIT, 2B4, and TIM-3 on helper T cells. Among co-stimulatory/activation markers, CD27 was upregulated, while 4-1BB was reduced in MGUS and NDMM in helper T cells. DNAM-1 was increased in the overall MM cohort and in both MMinTx and MMnoTx subgroups, and ICOS expression was elevated in MMnoTx compared with HD (Figure 3C).

In CTLs, inhibitory checkpoint molecules showed prominent upregulation of TIGIT and TIM-3 in MM, with increased LAG-3 in MGUS, MM, MMinTx, and MMnoTx. CTLA-4 was decreased in MMinTx, and PD-1 expression was reduced across all five MM stages; BTLA and 2B4 showed no
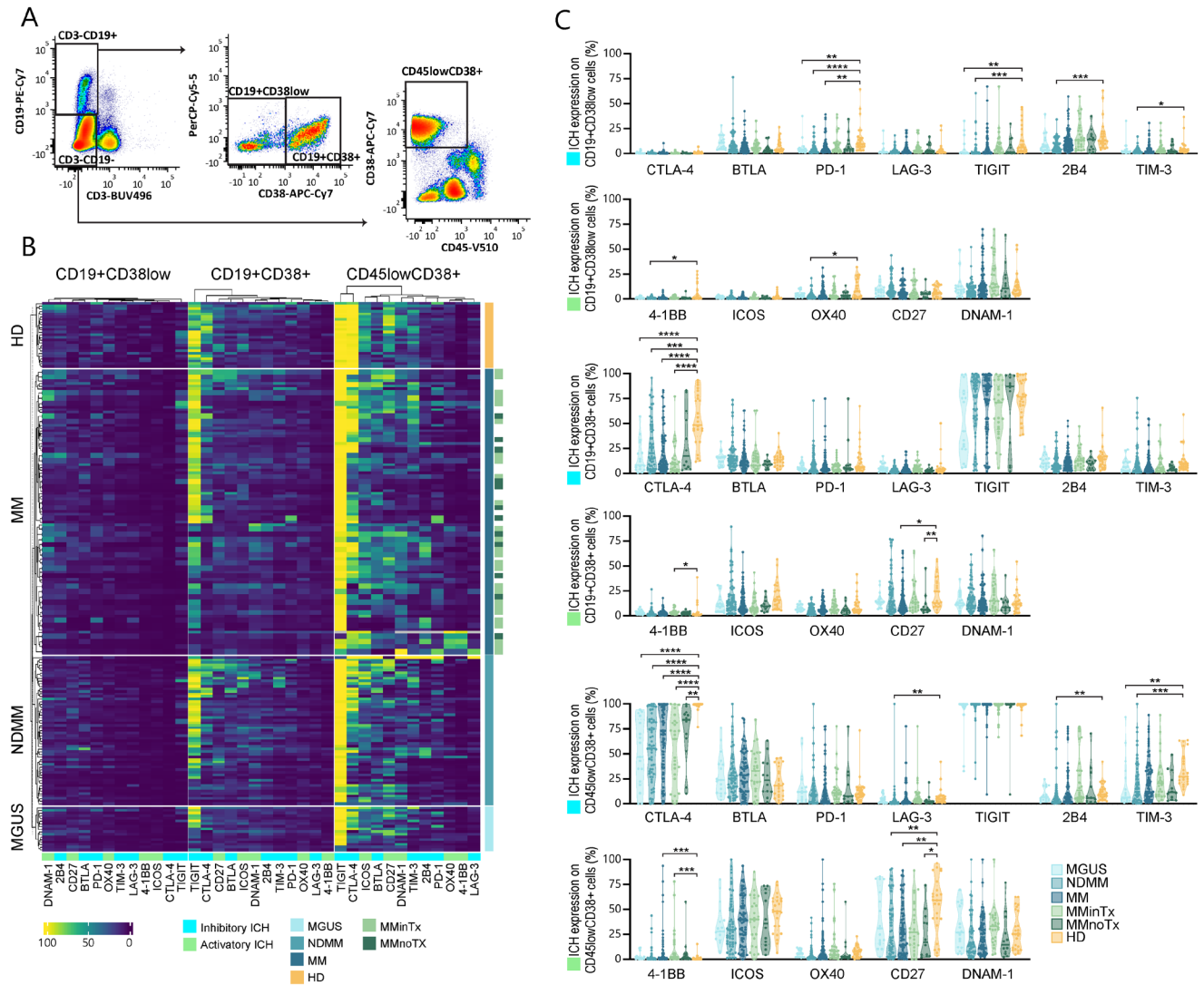
Figure 2. Immune checkpoint profiling of bone marrow B cell subsets across MM disease stages. (A) Gating strategy used to identify total B cells (CD19$^+$) and to define CD19$^+$CD38^{low} (mature naïve to memory B cells), CD19$^+$CD38$^+$ (activated/proliferating B cells), and CD19$^-$CD45^{low}CD38^{++} (plasmablasts/plasma cells). **(B)** Heatmap showing patient-level expression of inhibitory (PD-1, TIM-3, TIGIT, 2B4, CTLA-4, BTLA, LAG-3) and co-stimulatory (4-1BB, OX40, CD27, DNAM-1, ICOS) immune checkpoint receptors across B cell compartments (CD19$^+$CD38^{low}, CD19$^+$CD38$^+$, and CD19$^-$CD45^{low}CD38^{++}). Samples are ordered to display subgroup-specific expression patterns (groups as indicated). **(C)** Expression of inhibitory (PD-1, TIM-3, TIGIT, 2B4, CTLA-4, BTLA, LAG-3) and co-stimulatory (4-1BB, OX40, CD27, DNAM-1, ICOS) immune checkpoint receptors across B cell compartments (CD19$^+$CD38^{low}, CD19$^+$CD38$^+$, and CD19$^-$CD45^{low}CD38^{++}). Marker expression is shown as the percentage (%) of cells expressing specific markers within B cell compartments. Individual points represent donors, and horizontal lines indicate the median and interquartile range for each clinical group. Statistical comparisons between MM groups and HD were performed using Dunn's multiple comparison test following the Kruskal-Wallis one-way analysis of variance. Statistical significance is indicated as *p<0.05, **p<0.01, ***p<0.001, and ****p<0.0001.

consistent modulation. Among activation markers, 4-1BB was downregulated, whereas DNAM-1 was upregulated in CTLs across all MM stages; CD27 was selectively increased in MGUS, while ICOS and OX40 remained unchanged. CD3$^+$DN T cells exhibited increased CD27 in MGUS, decreased BTLA in MMinTx, and reduced 4-1BB in NDMM. CD3$^+$DP T cells showed downregulation of 4-1BB in NDMM and upregulation of CTLA-4 in NDMM, with no significant changes in ICOS and OX40. Overall, MM is associated with

subset-specific reprogramming of T cell immune checkpoints, characterized by decreased PD-1, selective upregulation of alternative inhibitory receptors (TIM-3, TIGIT, LAG-3, BTLA), and a mixed pattern of co-stimulatory marker changes (CD27, DNAM-1, 4-1BB) that differ between helper T cells, CTLs, CD3$^+$DN, and CD3$^+$DP T cell populations, as well as between treatment-status subgroups.

Checkpoint remodeling of NKT cells across MM stages. NKT cells were identified as CD3$^+$CD56$^+$ events
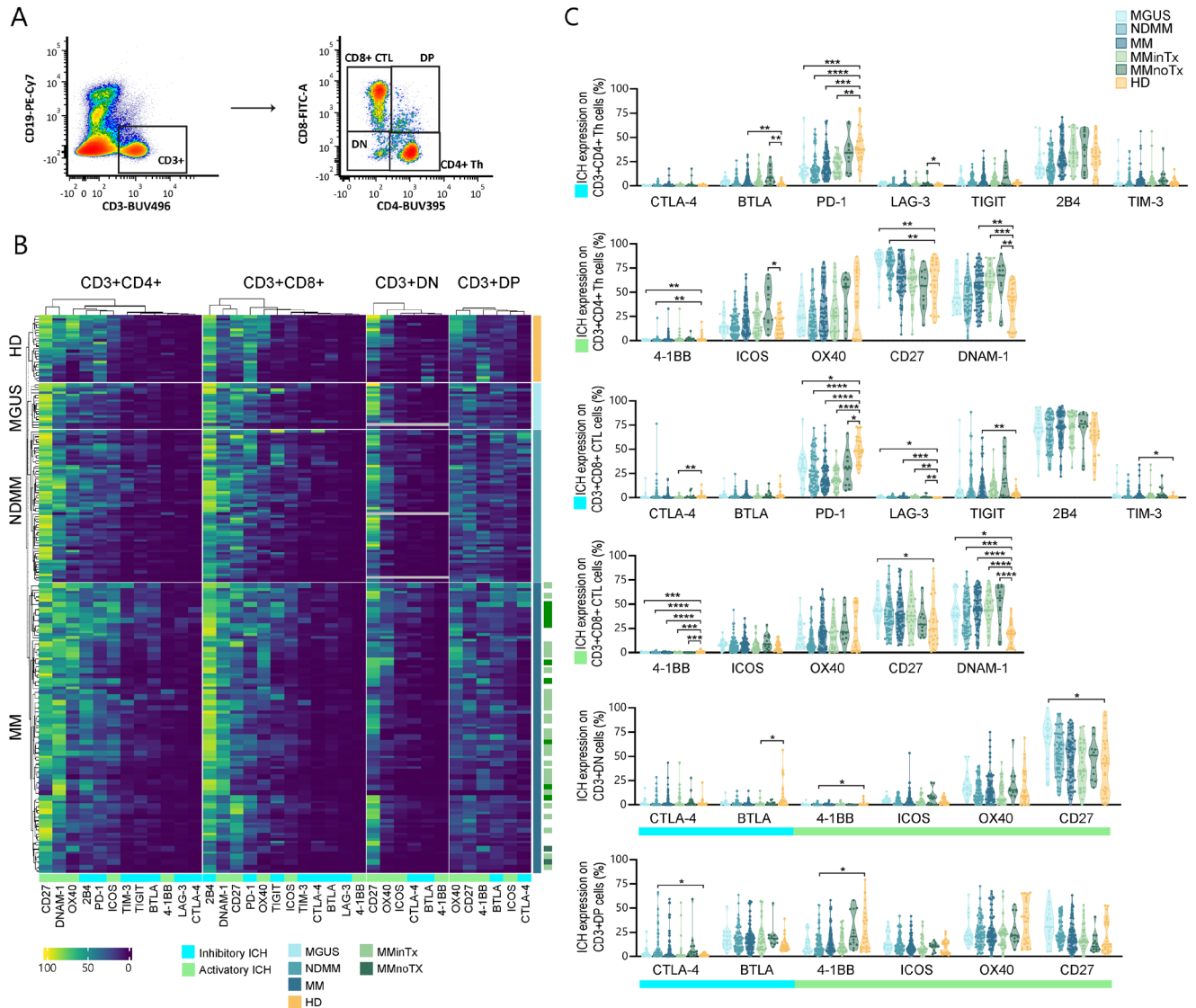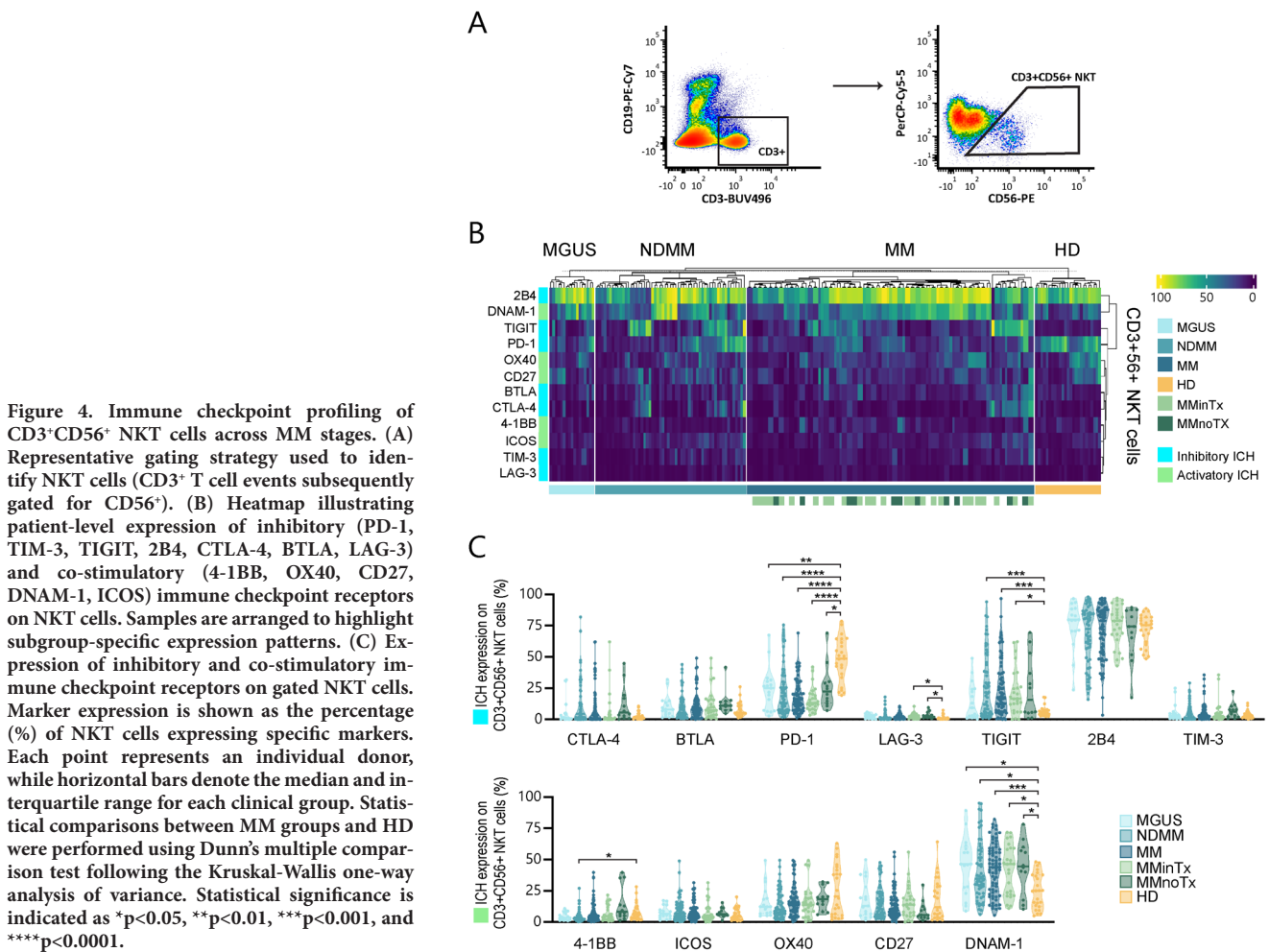
Figure 3. Subset-specific modulation of immune checkpoint receptors in T cells across MM disease stages. (A) Representative gating strategy used to identify adaptive T cell populations. Total CD3$^+$ lymphocytes were gated and subsequently resolved into CD4$^+$ helper T cells, CD8$^+$ cytotoxic T lymphocytes (CTLs), double-negative (DN; CD3$^+$CD4$^-$CD8$^-$), and double-positive (DP; CD3$^+$CD4$^+$CD8$^+$) T subsets. **(B)** Heatmap showing patient-level expression of inhibitory (PD-1, TIM-3, TIGIT, 2B4, CTLA-4, BTLA, LAG-3) and co-stimulatory (4-1BB, OX40, CD27, DNAM-1, ICOS) immune checkpoint receptors across T cell compartments (helper T cells, CTLs, CD3$^+$DN, and CD3$^+$DP cells). **(C)** Subset-specific expression of inhibitory (PD-1, TIM-3, TIGIT, 2B4, CTLA-4, BTLA, LAG-3) and stimulatory (4-1BB, OX40, CD27, DNAM-1, ICOS) immune checkpoint receptors within T cell compartments. Marker expression is presented as the percentage (%) of T cells expressing the respective markers. Individual points represent donors, and horizontal lines indicate the median and interquartile range for each clinical group. Statistical comparisons between MM groups and HD were performed using Dunn's multiple comparison test following the Kruskal-Wallis one-way analysis of variance. Statistical significance is denoted as *p<0.05, **p<0.01, ***p<0.001, and ****p<0.0001.

after sequential gating on CD3$^+$ T cells and CD56$^+$ cells (Figure 4A). The frequency of NKT cells showed no significant difference among the five MM stages and HD (Supplementary Figure S2C). A heatmap illustrating the relative median expression of inhibitory and stimulatory immune-checkpoint molecules across individual patients and clinical cohorts (HD and five MM stages) reveals distinct checkpoint modulation patterns within NKT cells (Figure 4B).

Analysis of checkpoint receptors on the NKT population revealed a significant reduction in PD-1 expression across all MM stages relative to HD. By contrast, TIGIT was significantly upregulated in the NDMM, MM, and MMinTx groups, and LAG-3 expression was increased in MMinTx and MMnoTx, whereas CTLA-4, BTLA, and TIM-3 showed no consistent change across the groups (Figure 4C). With respect to co-stimulatory receptors, 4-1BB expression was

Figure 4. Immune checkpoint profiling of CD3⁺CD56⁺ NKT cells across MM stages. (A) Representative gating strategy used to identify NKT cells (CD3⁺ T cell events subsequently gated for CD56⁺). (B) Heatmap illustrating patient-level expression of inhibitory (PD-1, TIM-3, TIGIT, 2B4, CTLA-4, BTLA, LAG-3) and co-stimulatory (4-1BB, OX40, CD27, DNAM-1, ICOS) immune checkpoint receptors on NKT cells. Samples are arranged to highlight subgroup-specific expression patterns. (C) Expression of inhibitory and co-stimulatory immune checkpoint receptors on gated NKT cells. Marker expression is shown as the percentage (%) of NKT cells expressing specific markers. Each point represents an individual donor, while horizontal bars denote the median and interquartile range for each clinical group. Statistical comparisons between MM groups and HD were performed using Dunn's multiple comparison test following the Kruskal-Wallis one-way analysis of variance. Statistical significance is indicated as *p<0.05, **p<0.01, ***p<0.001, and ****p<0.0001.

significantly decreased at the NDMM stage. Conversely, DNAM-1 expression was increased across all five MM stages compared with HD, while ICOS, OX40, and CD27 expression on NKT cells remained unchanged (Figure 4C). Overall, MM is associated with a loss of NKT cells and a remodeling of their immune-checkpoint profile, marked by decreased PD-1 and 4-1BB, increased TIGIT and DNAM-1, and selective upregulation of LAG-3, consistent with a shift toward alternative inhibitory pathways and altered co-stimulatory signaling.

Immune checkpoints remodel γ/δ T cell phenotype in MM. To interrogate the interface between innate and adaptive immunity, we profiled γ/δ T cells. γ/δ T cells were identified by gating CD45⁺CD3⁺ events and subsequently selecting TCR γ/δ⁺ cells (CD3⁺TCRγδ⁺) (Figure 5A). The frequency of γ/δ T cells did not differ significantly among groups compared with HD (Supplementary Figure S2D). A heatmap of LST1-panel markers (CTLA-4, BTLA, 4-1BB, ICOS, OX40, and CD27) displays patient-level checkpoint expression patterns (Figure 5B). At the receptor level, we

observed a significant reduction in the inhibitory receptors CTLA-4 and BTLA specifically in the MMinTx subgroup compared with HD (Figure 5C). Among stimulatory receptors, OX40 expression was significantly decreased in the NDMM and MM patient groups, including MMinTx, relative to HD, whereas 4-1BB, ICOS, and CD27 showed no significant modulation across disease stages (Figure 5C). Collectively, these data reveal selective downregulation of inhibitory (CTLA-4, BTLA) and co-stimulatory (OX40) receptors on γ/δ T cells at defined MM stages, despite preserved γ/δ T cell frequencies.

NK cell immune checkpoint signatures in MM. NK cells were identified as CD3⁻CD56⁺ events by sequential gating on CD3⁻ lymphocytes followed by selection of CD56⁺ cells (Figure 6A). Compared with HD, the frequency of NK cells was significantly reduced in the MM cohort and specifically in the MMinTx subgroup (Supplementary Figure S2E). A heatmap representation of checkpoint receptor expression across the whole cohort, comprising seven inhibitory and five stimulatory receptors, revealed clear clustering by MM
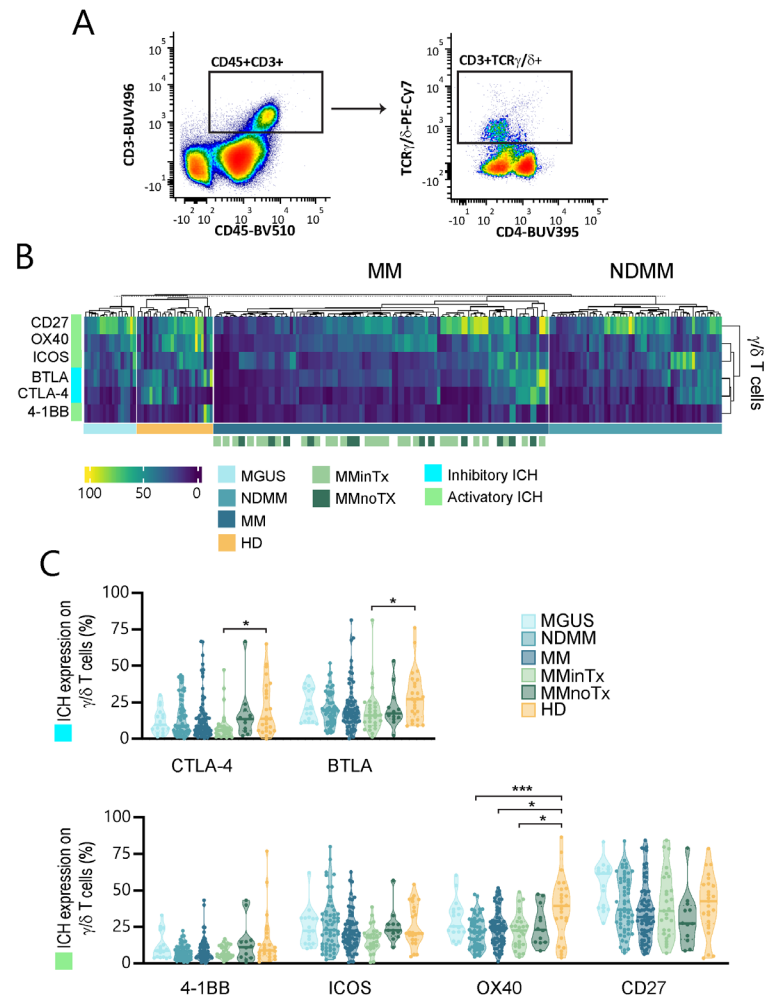
Figure 5. Immune checkpoint expression on γδ T cells across MM stages. (A) Representative gating strategy used to identify γδ T cells; CD3⁺ events gated for TCRγ/δ (CD3⁺TCRγδ⁺). **(B)** Heatmap showing patient-level expression from the LST1 panel, including CTLA-4, BTLA, 4-1BB, ICOS, OX40, and CD27 on γδ T cells. Samples are ordered to reveal subgroup-specific expression trends. **(C)** Expression of inhibitory (CTLA-4, BTLA) and stimulatory (4-1BB, ICOS, OX40, CD27) checkpoint receptors on γδ T cells. Marker expression is presented as the percentage (%) of γδ T cells expressing each receptor. Individual points correspond to donors, with horizontal lines indicating the group median and interquartile range. Statistical comparisons between MM groups and HD were conducted using Dunn's multiple comparison test following the Kruskal-Wallis one-way analysis of variance. Statistical significance is shown as *p<0.05, **p<0.01, ***p<0.001, and ****p<0.0001.

subgroup (Figure 6B), indicating subgroup-specific checkpoint repertoires. Profiling of inhibitory checkpoint receptors on NK cells showed a consistent and significant downregulation of TIM-3 across all five MM stages. PD-1 expression was significantly decreased in MGUS, NDMM, MM, and MMinTx compared with HD. In contrast, TIGIT expression was elevated in NDMM and MM, and 2B4 was increased in MGUS, MM, and MMinTx. No significant differences were detected for CTLA-4, BTLA, or LAG-3 (Figure 6C). Assessment of stimulatory (co-stimulatory/activating) receptors revealed significantly reduced expression of 4-1BB and OX40 in NDMM, with 4-1BB also decreased in MM and MMinTx relative to HD. By contrast, DNAM-1 was upregulated in MGUS, NDMM, MM, and MMinTx. Expression of ICOS and CD27 did not differ significantly between groups (Figure 6C). Together, these data demonstrate a stage-dependent remodeling of the NK cell immune-checkpoint landscape in MM, characterized by a concurrent loss of several activating receptors and selective alterations among inhibitory receptors that vary by disease stage.

Immune checkpoint expression in B and T cell subsets predicts PFS in MM. To identify risk factors for disease progression among all patients, we fitted a multivariable Cox proportional hazards model that revealed differential expression of several immune checkpoints, including TIGIT in mature naïve/memory B cells (CD19⁺CD38^low), CTLA-4 in plasmablasts/plasma cells (CD45^lowCD38⁺) and in CD3⁺DN T cells, OX40 in plasmablasts/plasma cells, and ICOS in CD3⁺DN T cells, as predictors of PFS (Figure 7). When comparing patients stratified into low- and high-expression groups relative to HD from our cohort, low TIGIT expression in mature naïve/memory B cells was strongly associated with improved PFS (p=0.0001). Likewise, reduced CTLA-4 expression in plasmablasts/plasma cells correlated with better PFS (p=0.0213). By contrast, higher OX40 expression within plasmablasts/plasma cells was linked to superior PFS (p=0.0174). Within the CD3⁺DN T cell compartment, low levels of CTLA-4 and ICOS were both significantly associated with favorable PFS (p=0.0282 and p=0.0118, respectively). Collectively, these findings suggest that distinct checkpoint

expression profiles across B cell and T cell subsets may hold prognostic value and reflect differential immunoregulatory pressures within the MM microenvironment.

Discussion

By applying high-dimensional, subset-resolved flow cytometry to BM immune cells across the continuum from MGUS to newly diagnosed and relapsed MM, we comprehensively characterized inhibitory and co-stimulatory checkpoint expression within the tumor microenvironment. Mapping checkpoint expression across B-cell maturation stages, distinct T-cell compartments, and innate effectors reveals potential axes of immune dysregulation and immune escape that bulk analyses may miss. These data provide a rational framework for prioritizing checkpoint targets and combination strategies for functional validation and clinical translation, and underscore the need to consider both inhibitory and activating receptor networks when designing immunotherapeutic interventions in MM.

Inhibitory immune-checkpoint receptors, including PD-1, TIM-3, TIGIT, and 2B4, are frequently dysregulated in MM and cooperate in shaping an immunosuppressive BM niche. PD-1 is upregulated on CD4+ and CD8+ T cells in the BM and blood, correlating with tumor burden, disease progression, and poor outcome. PD-1 ligands (PD-L1/PD-L2) are variably expressed on malignant and microenvironmental cells, further reinforcing local immune suppression [21, 22]. TIM-3, expressed on exhausted T cells, Tregs, NK, and myeloid cells, is also aberrantly present on malignant plasma cells in MM and associates with β2-microglobulin levels, disease progression, and worse prognosis. Mechanistic studies implicate TIM-3-NF-κB signaling in MM proliferation and survival, while knockdown induces apoptosis [23, 24]. TIGIT is frequently co-expressed with PD-1 and TIM-3 on dysfunctional effector-memory and terminally differentiated CD8+ cells in MM and is also found on MDSCs and occasionally tumor cells. By binding CD155/CD112 and competing with the activating receptor DNAM-1, TIGIT promotes inhibitory signaling and correlates with aggressive
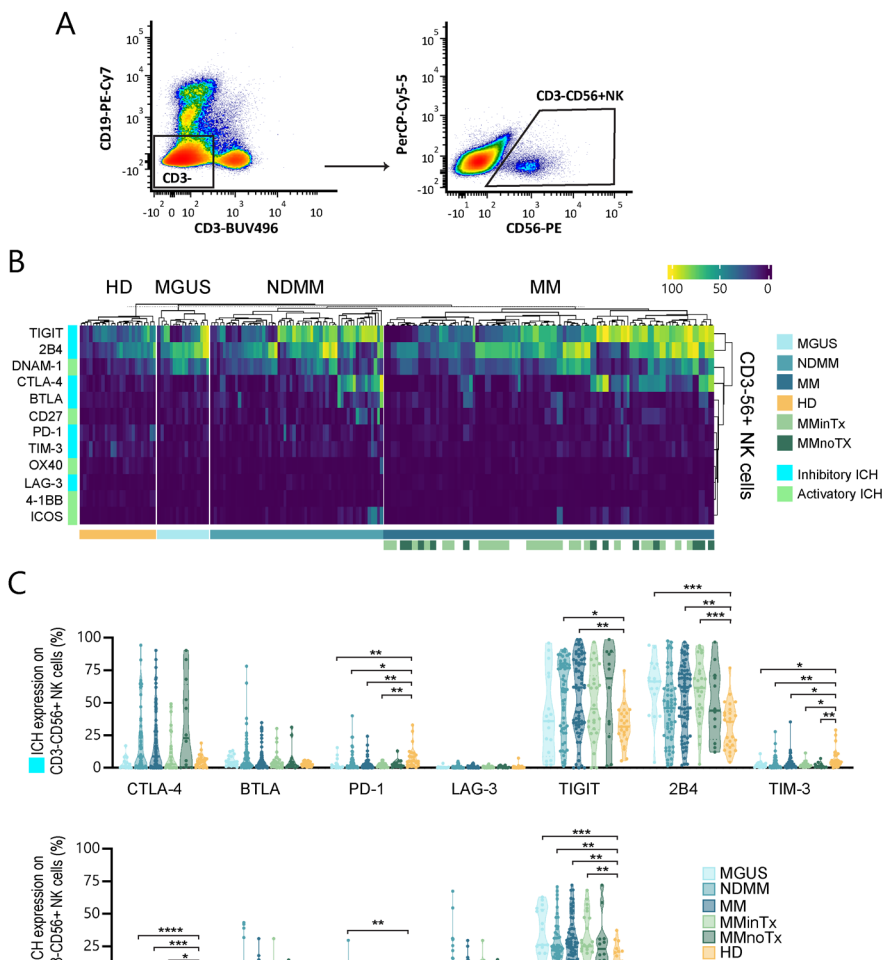

Figure 6. Immune checkpoint profiling of NK cells across MM stages. (A) Representative gating strategy for NK cells (CD3−CD56+), with example plots showing CD3− events further gated on CD56+ cells. (B) Heatmap depicting expression levels of inhibitory (PD-1, TIM-3, TIGIT, 2B4, CTLA-4, BTLA, LAG-3) and co-stimulatory (4-1BB, OX40, CD27, DNAM-1, ICOS) immune checkpoint receptors on NK cells across the entire cohort. Samples are clustered according to MM subgroups. (C) Expression of inhibitory (PD-1, TIM-3, TIGIT, 2B4, CTLA-4, BTLA, LAG-3) and stimulatory (4-1BB, OX40, CD27, DNAM-1, ICOS) checkpoint receptors on NK cells. Marker expression is shown as the percentage (%) of NK cells expressing the specific markers. Each symbol denotes an individual donor; horizontal bars indicate the median and interquartile range for each group. Statistical comparisons between MM groups and HD were performed using Dunn's multiple comparisons test following Kruskal-Wallis one-way analysis of variance. Statistical significance is indicated as *p<0.05, **p<0.01, ***p<0.001, and ****p<0.0001.
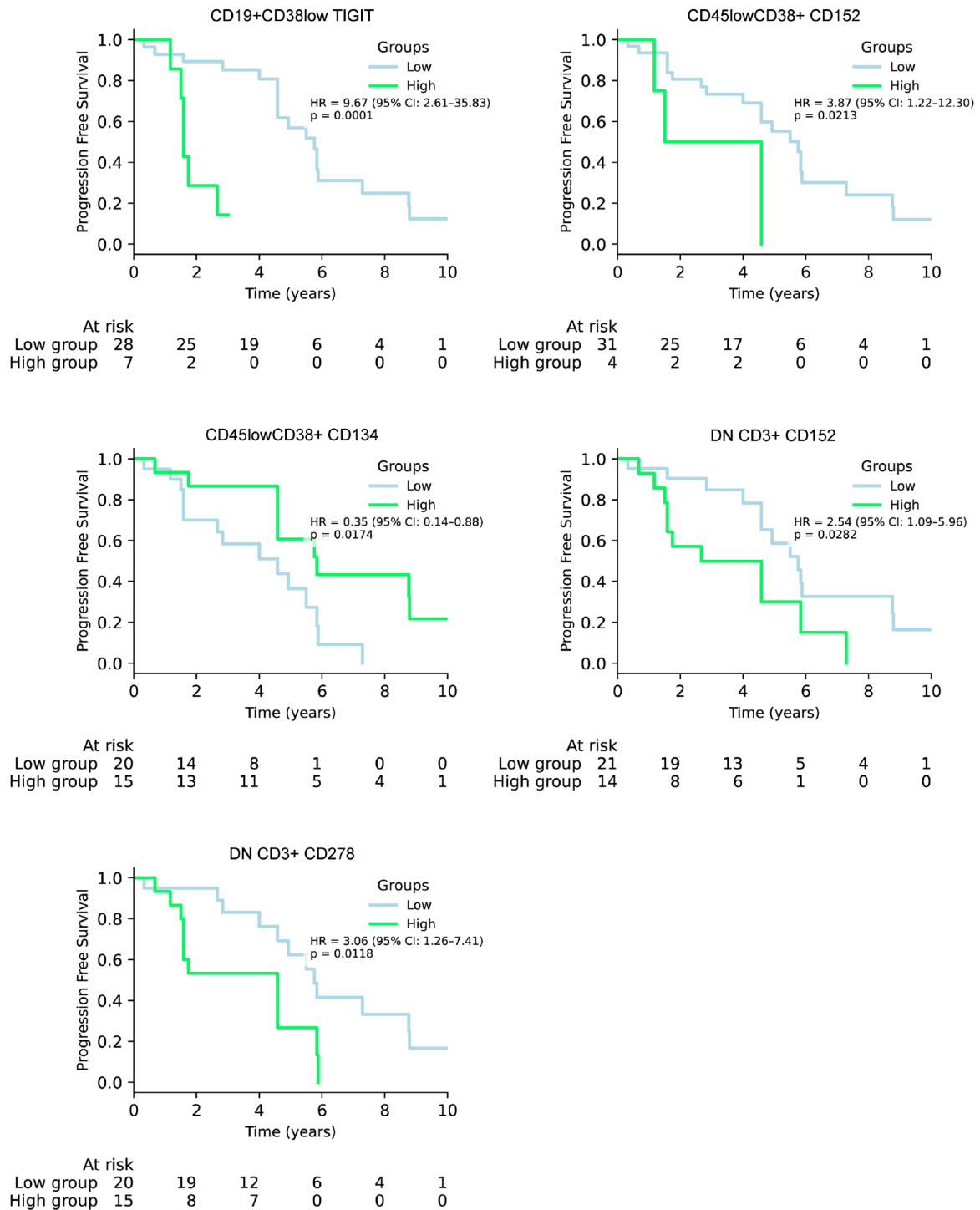
Figure 7. Kaplan-Meier estimates of PFS stratified by immune checkpoint expression. Kaplan-Meier curves display PFS for patients grouped into low- and high-expression categories for individual immune checkpoints, with expression thresholds defined relative to healthy donor reference levels from our cohort. Panels show TIGIT in mature naïve/memory B cells (CD19+CD38low), CTLA-4 in plasmablasts/plasma cells (CD45lowCD38+), OX40 in plasmablasts/plasma cells, CTLA-4 in CD3+DN T cells, and ICOS in CD3+DN T cells. Group comparisons were performed using the log-rank test, and associated p-values are reported on each panel. Hazard ratios (HRs) and 95% confidence intervals (CIs), estimated using Cox proportional-hazards models, are indicated on the corresponding panels, and the number of patients at risk is provided beneath each curve. Statistical significance was defined as p<0.05.

disease [25, 26]. 2B4 (CD244), present on NK cells, a subset of CD8+ T cells, DCs, and MDSCs, marks exhausted CD8+ cells and mediates inhibitory NK signaling with reduced proliferation and cytotoxicity. Its downstream outcome depends on SAP adaptor levels, such that high 2B4 with low SAP favors inhibitory signaling. 2B4 has also been reported on tumor cells, where its knockdown impairs proliferation, suggesting a dual immune-tumor role [27]. CTLA-4, BTLA, and LAG-3 are additional components of MM's dysfunctional immune landscape. CTLA-4 is elevated on CD8+ T cells (often co-expressed with PD-1, CD160, and ICOS) and on Tregs and circulating T_FH subsets, reinforcing an immunosuppressive niche. Tumor plasma cells express little CTLA-4 but can modulate checkpoint expression on immune cells [10, 28]. Multi-omics analyses link CTLA-4 with PD-1 and TIGIT networks, define CXCL9+ immune-activated subgroups, and highlight dysfunctional CD8+ and regulatory populations; CTLA-4 polymorphisms correlate with clinical outcomes and may aid patient stratification [29, 30]. BTLA is variably expressed on exhausted CD8+ cells, Tregs, B cells, and occasionally plasma cells, co-existing with PD-1 and LAG-3 and signaling via the BTLA-HVEM axis [31, 32]. LAG-3 is upregulated on activated/exhausted CD4+ and CD8+ T cells, Tregs, NK cells, B cells, and pDCs (including MGUS) and is linked to impaired proliferation, cytokine secretion, and cytotoxicity. Mechanistically, LAG-3 dampens TCR signaling via its KIEELE motif and binds both MHC-II and non-MHC ligands (Galectin-3, LSECtin), broadening its inhibitory scope [33, 34]. Clinically, checkpoint blockade in MM shows limited single-agent activity (notably PD-1 and CTLA-4), but combination approaches, particularly PD-1 with IMiDs, and next-generation targets show promise. TIM-3 inhibition (e.g., sabatolimab) demonstrates acceptable safety and T cell reinvigoration; LAG-3 and BTLA antagonists show early clinical activity; and 2B4 strategies are advancing in CAR-NK and NK platforms. Meanwhile, CTLA-4 combinations (with PD-1/IMiDs, TIGIT/LAG-3 inhibitors, CAR-T, or bispecifics) report some immune responses yet raise toxicity concerns [22, 35–39]. Together, these data highlight coordinated checkpoint dysregulation and support rational combinatorial regimens, while emphasizing the need for predictive biomarkers and vigilant safety evaluation to balance efficacy with immune-related toxicity.

Co-stimulatory receptors and activation pathways, including CD137 (4-1BB), ICOS, OX40, CD226, and CD27, bolster T and NK cell activation, proliferation, and cytotoxicity within the myeloma microenvironment. CD137 (4-1BB) is expressed on activated T and NK cells and is linked to immune activation, T cell proliferation, survival, and cytotoxicity; 4-1BB stimulation can partially restore impaired CD8+ T cell function in MM [40, 41]. ICOS (CD278), highly expressed on activated T cells (notably T_FH), is abundant in the MM TME and, via ICOSL on APCs and tumor cells, modulates helper cytokine production (IL-10, IL-4) and Treg function, with variable prognostic associations [42, 43].

OX40 (CD134), a TNFR-family co-stimulatory receptor on activated T and NK cells, is upregulated with T cell activation in MM, promotes T-cell survival, proliferation, and memory, and OX40-containing CAR-T constructs increase persistence and antitumor activity in MM models [44–46]. DNAM-1 (CD226) binds tumor-expressed CD155/CD112 to drive NK- and CD8+-mediated cytotoxicity, but its function is antagonized by TIGIT, CD96, and PVRIG and can be lost during progression; conversely, standard myeloma treatments may transiently increase CD155/CD112 and sensitize tumor cells to CD226-mediated killing [47]. CD27–CD70 signaling further modulates immune–tumor crosstalk (including PERK/ATF4-linked pathways). CD27 is expressed on T and B cells and variably on malignant plasma cells in MM; loss of CD27 on plasma cells is associated with higher-risk disease, while CD27 expression shows context-dependent prognostic implications [48–50]. Next-generation strategies harness co-stimulatory axes to enhance antimyeloma immunity: tumor-selective bispecific 4-1BB agonists and 4-1BB-containing CAR-T cells (e.g., BCMA, CD19) have produced partial responses or stable disease with acceptable safety, whereas ICOS and OX40 agonists (including OX40-enhanced CAR-T), particularly combined with checkpoint blockade, induce immune activation but limited single-agent efficacy, supporting combinatorial approaches [42, 44–46, 51]. Direct CD226 agonism has encountered setbacks, redirecting focus to the broader CD226/TIGIT/PVR axis and to CD226-engineered NK/T-cell therapies. CD27/CD70-targeted CARs and antibody platforms show promising preclinical activity and are entering early clinical testing in MM [52–54]. Together, these complementary co-stimulatory axes are attractive therapeutic targets but require strategies that preserve effector function while avoiding compensatory inhibitory mechanisms.

In our previous study, we demonstrated that B cell lymphopoiesis is progressively disrupted across disease stages, with significant reductions in B cell progenitors, immature, transitional, and unswitched memory B cells in SMM and active MM, whereas switched memory B cells and plasmablasts were already elevated at the MGUS stage and further expanded in SMM and NDMM [12]. Furthermore, we identified dysregulated B-cell development in MM, characterized by the upregulation of key signaling (MMSET, MYD88, c-Myc, Notch1) and stemness (Nanog, KLF4, Oct3/4, Sox2) factors, along with aberrant expression of B-cell and plasma-cell regulators within the BM microenvironment [55]. In this study, we observed a consistent reduction of mature naïve-to-memory and activated/proliferating B cell subsets across multiple disease stages, together with an NDMM-specific expansion of plasmablasts/plasma cells, indicating a shift toward terminal B cell differentiation in early symptomatic disease. In parallel, alterations in immune checkpoint expression further suggest that B cell maturation and differentiation in MM are accompanied by remodeling of their regulatory receptor landscape. Notably, reduced PD-1,

TIM-3, TIGIT, and 2B4 on mature B cells, and decreased CTLA-4 on activated B cells and plasmablasts/plasma cells, point to a global alteration of inhibitory signaling that may influence antigen responsiveness, survival, or interactions with T cells and other marrow immune components. Importantly, this pattern also carries clinical relevance, as low TIGIT expression in mature B cells was strongly associated with improved PFS, while reduced CTLA-4 on plasmablasts/plasma cells similarly correlated with better PFS. By contrast, higher OX40 expression within plasmablasts/plasma cells was linked to superior PFS, further supporting the idea that perturbing these immune checkpoint circuits may enhance antitumor immunity and contribute to more effective disease control. Within the plasmablast/plasma cell compartment, TIM-3 expression was decreased in MGUS and NDMM, while LAG-3 and 2B4 were specifically reduced in NDMM. OX40 expression on mature B cells was also downregulated in NDMM. The selective downregulation of CD27 on plasmablasts/plasma cells and activated B cells, together with the divergent regulation of 4-1BB, decreased in naïve to memory B cells at NDMM but increased on plasmablasts/plasma cells in MM and MMinTx, indicates that co-stimulatory pathways are engaged in a stage- and differentiation-dependent manner. Taken together, these findings indicate that immune checkpoint programs in B cells are dynamically rewired during MM evolution in a manner that may impact humoral function and local immune regulation. These observations warrant functional studies to determine whether the identified receptor alterations affect B cell signaling, antibody production, or responsiveness to immunomodulatory therapies, and whether specific checkpoint signatures could serve as biomarkers of disease progression or therapeutic response.

Our profiling of NK cells reveals a complex, stage-dependent reorganization of checkpoint receptor expression that likely contributes to NK-cell dysfunction in MM. As MM progresses to active disease, NK-cell frequencies in both BM and peripheral blood decline, with a pronounced loss of activated NK-cell subsets [56]. Similarly, we observed that the reduction in NK-cell frequency in the MM stage, and specifically in the MMinTx subgroup, may indicate a quantitative impairment that underlies functional defects. Concomitant downregulation of TIM-3 (CD366) across stages and decreased PD-1 (CD279) in several stages likely reflects loss or phenotypic alteration of activated NK subsets rather than restored function; reduced surface expression of canonical exhaustion markers can result from selective depletion of marker-positive cells or receptor internalization and should not be interpreted solely as reduced exhaustion [23, 28, 57]. By contrast, stage-specific upregulation of inhibitory receptors such as TIGIT and 2B4 (CD244) indicates engagement of alternative inhibitory pathways during progression. Concurrent loss of co-stimulatory receptors (notably 4-1BB/CD137 and OX40/CD134), particularly in NDMM and later stages, provides an additional mechanism limiting NK-cell cytotoxic potential by reducing responsiveness to stress or antibody-coated targets. The observed increase in DNAM-1 across several patient groups may reflect compensatory expansion of DNAM-1+ subsets or altered subset composition; whether this preserves cytotoxicity or signals dysfunctional activation amid opposing inhibitory cues remains unclear. Collectively, these data indicate that NK-cell dysregulation in MM is not a uniform exhaustion program but a selective rewiring of activating and inhibitory receptor networks that varies with disease stage. This has therapeutic implications, as stage-tailored blockade of specific inhibitory axes (e.g., TIGIT) or restoration of co-stimulatory signaling (e.g., 4-1BB agonists) may be beneficial, although receptor downregulation and altered subset composition could affect treatment efficacy.

Within the T cell compartment, CD8+ naïve and effector subsets were reduced in SMM, NDMM, and RRMM but preserved in MGUS, whereas CD4+ central and effector memory subsets were expanded in the more advanced stages [12]. In this cohort, the expansion of CD4+ helper T cells in MGUS and NDMM alongside a selective reduction of CD8+ CTLs in MGUS suggests an early skewing of the adaptive compartment that precedes or accompanies disease progression. Moreover, our data reveal a complex, subset-specific reshaping of T-cell immune checkpoints across the MGUS-MM spectrum. Checkpoint profiling shows a relative reduction of PD-1 across multiple MM stages that contrasts with selective increases in alternative inhibitory receptors, notably LAG-3, TIM-3, and TIGIT on CTLs, and BTLA and LAG-3 on helper T cells (with CTLA-4 also increased on CD3+ DP cells), pointing to a shift from canonical PD-1–mediated regulation toward alternative suppressive pathways. Within the CD3+ DN T cell compartment, lower expression of CTLA-4 and ICOS was significantly linked to improved PFS, highlighting the potential prognostic relevance of inhibitory and co-stimulatory signaling in this subset. Concomitant changes in co-stimulatory markers indicate a heterogeneous activation landscape: upregulation of CD27 (on CTLs, helper T cells, and CD3+ DN cells), DNAM-1 (on CTLs and helper T cells), and ICOS (on helper T cells) in some subsets may reflect compensatory activation or an altered co-stimulatory balance, whereas consistent downregulation of 4-1BB across subgroups (CTLs, helper T cells, CD3+ DN, and CD3+ DP cells) could reduce responsiveness to 4-1BB agonism. Furthermore, the frequency of NKT cells did not differ significantly across MM stages, but their checkpoint landscape was notably reconfigured. The decreased PD-1 expression on NKT cells suggests PD-1 downregulation is not the dominant inhibitory axis in these cells during MM progression. Instead, consistent TIGIT upregulation (in NDMM, MM, and MMinTx) and selective increases in LAG-3 (in MMinTx and MMnoTx) point to engagement of alternative inhibitory pathways that may impair NKT function or alter subset composition. The concurrent increase in DNAM-1 across MM stages, together with a stage-specific decrease in the co-stimulatory receptor 4-1BB at NDMM, further indicates complex rewiring of

activating and inhibitory signals, potentially reflecting enrichment of phenotypically distinct NKT subsets or compensatory receptor modulation in response to the tumor microenvironment. Profiling of γ/δ T cells revealed a marked decrease in the inhibitory receptors CTLA-4 and BTLA in MM patients undergoing treatment (MMinTx), together with downregulation of the co-stimulatory receptor OX40 in NDMM and MM, suggesting treatment- and stage-associated reshaping of γ/δ T cell phenotypes. Because γ/δ T cell frequencies were preserved, these changes likely reflect phenotypic reprogramming or selective loss of specific functional subsets rather than simple depletion. In summary, these findings indicate early adaptive skewing (CD4$^+$ expansion with CD8$^+$ CTL reduction), a stage-specific shift from PD-1 to alternative inhibitory receptors, heterogeneous alterations in co-stimulatory signaling, and phenotypic modification of non-classical T cells (NKT and γ/δ T), all of which point to multifaceted immune dysfunction that could inform tailored immunotherapeutic strategies.

In summary, our data show that immune checkpoint programs are selectively and dynamically remodeled across B cells, NK cells, T cells (including NKT and γ/δ T subsets) during MM evolution and disease progression, rather than reflecting a uniform exhaustion state. This receptor- and subset-specific remodeling, highlighted by the prominence of TIGIT, TIM-3, and LAG-3 as well as shifts in DNAM-1, 4-1BB, and other axes, includes several checkpoints with prognostic relevance. Checkpoint alterations demonstrating distinct associations with clinical outcomes, such as low TIGIT or CTLA-4 expression and elevated OX40 expression, underscore heterogeneous prognostic effects that may constrain single-agent checkpoint strategies. To prioritize targets and rational combinations, functional validation (including ligand engagement, cytokine release, cytotoxicity, and proliferation assays), longitudinal sampling, and correlation with clinical outcomes will be essential to distinguish causal drivers of dysfunction from compensatory or correlative changes. Ultimately, these follow-up studies should define checkpoint signatures that serve both as biomarkers of progression or response and as the basis for stage- and treatment-tailored immunomodulatory strategies.

Supplementary information is available in the online version of the paper.

References

[1] GAY F, MARCHETTI E, BERTUGLIA G. Multiple Myeloma Unpacked. Hematol Oncol 2025; 43 Suppl 2: e70067. https://doi.org/10.1002/hon.70067

[2] AVET-LOISEAU H, DAVIES FE, SAMUR MK, CORRE J, D'AGOSTINO M et al. International Myeloma Society/International Myeloma Working Group Consensus Recommendations on the Definition of High-Risk Multiple Myeloma. J Clin Oncol 2025; 43: 2739–2751. https://doi.org/10.1200/JCO-24-01893

[3] DIMOPOULOS MA, TERPOS E, BOCCADORO M, MOREAU P, MATEOS MV et al. EHA-EMN Evidence-Based Guidelines for diagnosis, treatment, and follow-up of patients with multiple myeloma. Nat Rev Clin Oncol 2025; 22: 680–700. https://doi.org/10.1038/s41571-025-01041-x

[4] CRISTOBAL-VARGAS S, CUADRADO M, GUTIERREZ NC. MYC alterations in multiple myeloma: Genetic insights and prognostic impact. Neoplasia 2025; 66: 101177. https://doi.org/10.1016/j.neo.2025.101177

[5] FOTIOU D, KATODRITOU E. From Biology to Clinical Practice: The Bone Marrow Microenvironment in Multiple Myeloma. J Clin Med 2025; 14: https://doi.org/10.3390/jcm14020327

[6] KAMAL M, SHISHIDO SN, MASON J, PATEL K, MANASANCH EE et al. Single-cell proteomic analysis reveals Multiple Myeloma heterogeneity and the dynamics of the tumor immune microenvironment in precursor and advanced states. Neoplasia 2025; 66: 101189. https://doi.org/10.1016/j.neo.2025.101189

[7] PORTUGUESE AJ, BANERJEE R, CHEN G, REDDI S, COWAN AJ. Novel Treatment Options for Multiple Myeloma. JCO Oncol Pract 2025; 21: 950–961. https://doi.org/10.1200/OP-24-00752

[8] DESANTIS V, SAVINO FD, SCARINGELLA A, POTENZA MA, NACCI C et al. The Leading Role of the Immune Microenvironment in Multiple Myeloma: A New Target with a Great Prognostic and Clinical Value. J Clin Med 2022; 11: https://doi.org/10.3390/jcm11092513

[9] FANG CF, LI Y, YANG C, FANG H, LI C. Bioinformatics analysis of intrinsic drivers of immune dysregulation in multiple myeloma to elucidate immune phenotypes and discover prognostic gene signatures. Sci Rep 2025; 15: 15662. https://doi.org/10.1038/s41598-025-00074-7

[10] CHENG Y, SUN F, ALAPAT DV, WANCHAI V, MERY D et al. Multi-omics reveal immune microenvironment alterations in multiple myeloma and its precursor stages. Blood Cancer J 2024; 14: 194. https://doi.org/10.1038/s41408-024-01172-x

[11] ZAVIDIJ O, HARADHVALA NJ, MOUHIEDDINE TH, SKLAVENITIS-PISTOFIDIS R, CAI S et al. Single-cell RNA sequencing reveals compromised immune microenvironment in precursor stages of multiple myeloma. Nat Cancer 2020; 1: 493–506. https://doi.org/10.1038/s43018-020-0053-3

[12] CHOLUJOVA D, BEKE G, KLUCAR L, DRGONA L, VALUSKOVA Z et al. CyTOF profiling of bone marrow immune dynamics across myeloma stages. Oncoimmunology 2025; 14: 2542333. https://doi.org/10.1080/2162402X.2025.2542333

[13] LUOMA S, SERGEEV P, JAVARAPPA KK, OHMAN TJ, VARJOSALO M et al. Deep Immune Profiling of Multiple Myeloma at Diagnosis and under Lenalidomide Maintenance Therapy. Cancers (Basel) 2023; 15: https://doi.org/10.3390/cancers15092604

[14] ZHAO Z, ZHAO Z, LIN Z, FAN L, XIAHOU Z et al. Decoding multiple myeloma: single-cell insights into tumor heterogeneity, immune dynamics, and disease progression. Front Immunol 2025; 16: 1584350. https://doi.org/10.3389/fimmu.2025.1584350

[15] OHLSTROM D, PILCHER WC, MICHAUD ME, ACHARYA CR, SATPATHY S et al. Longitudinal multi-omic profiling uncovers immune escape and predictors of response in multiple myeloma. bioRxiv 2025; 2025.2005.2027.656392. https://doi.org/10.1101/2025.05.27.656392

[16] WONG S, HAMIDI H, COSTA LJ, BEKRI S, NEPARIDZE N et al. Multi-omic analysis of the tumor microenvironment shows clinical correlations in Ph1 study of atezolizumab +/- SoC in MM. Front Immunol 2023; 14: 1085893. https://doi.org/10.3389/fimmu.2023.1085893

[17] XIE L, GAO M, TAN S, ZHOU Y, LIU J et al. A Monocyte-Driven Prognostic Model for Multiple Myeloma: Multi-Omics and Machine Learning Insights. Blood Lymphat Cancer 2025; 15: 21–37. https://doi.org/10.2147/BLCTT.S517354

[18] WANG J, ZHENG Y, TU C, ZHANG H, VANDERKERKEN K et al. Identification of the immune checkpoint signature of multiple myeloma using mass cytometry-based single-cell analysis. Clin Transl Immunology 2020; 9: e01132. https://doi.org/10.1002/cti2.1132

[19] BOTTA C, PEREZ C, LARRAYOZ M, PUIG N, CEDENA MT et al. Large T cell clones expressing immune checkpoints increase during multiple myeloma evolution and predict treatment resistance. Nat Commun 2023; 14: 5825. https://doi.org/10.1038/s41467-023-41562-6

[20] YE C, CHEN X, CHEN Z, LIU S, KONG R et al. Comprehensive analysis of single-cell and bulk RNA sequencing data reveals an EGFR signature for predicting immunotherapy response and prognosis in pan-cancer. Front Immunol 2025; 16: 1604394. https://doi.org/10.3389/fimmu.2025.1604394

[21] CHANG Y, JIANG Y, CHEN Y, XING X, ZHOU Y et al. Bone marrow PD-1 positive T cells reflect tumor mass and prognosis in multiple myeloma. Int J Clin Exp Pathol 2018; 11: 304–313.

[22] JELINEK T, PAIVA B, HAJEK R. Update on PD-1/PD-L1 Inhibitors in Multiple Myeloma. Front Immunol 2018; 9: 2431. https://doi.org/10.3389/fimmu.2018.02431

[23] JIANG W, LI F, JIANG Y, LI S, LIU X et al. Tim-3 Blockade Elicits Potent Anti-Multiple Myeloma Immunity of Natural Killer Cells. Front Oncol 2022; 12: 739976. https://doi.org/10.3389/fonc.2022.739976

[24] LIU Z, XIANG C, HAN M, MENG N, LUO J et al. Study on Tim3 Regulation of Multiple Myeloma Cell Proliferation via NF-kappaB Signal Pathways. Front Oncol 2020; 10: 584530. https://doi.org/10.3389/fonc.2020.584530

[25] CUI H, HAMAD M, ELKORD E. TIGIT in cancer: from mechanism of action to promising immunotherapeutic strategies. Cell Death Dis 2025; 16: 664. https://doi.org/10.1038/s41419-025-07984-4

[26] GUILLEREY C, HARJUNPAA H, CARRIE N, KASSEM S, TEO T et al. TIGIT immune checkpoint blockade restores CD8(+) T-cell immunity against multiple myeloma. Blood 2018; 132: 1689–1694. https://doi.org/10.1182/blood-2018-01-825265

[27] AGRESTA L, HOEBE KHN, JANSSEN EM. The Emerging Role of CD244 Signaling in Immune Cells of the Tumor Microenvironment. Front Immunol 2018; 9: 2809. https://doi.org/10.3389/fimmu.2018.02809

[28] VIG M, KUMAR L, DUBEY S, GUPTA R. Altered dynamics of T cell subsets in peripheral blood impacts disease progression in newly diagnosed multiple myeloma. Biochem Biophys Rep 2025; 43: 102104. https://doi.org/10.1016/j.bbrep.2025.102104

[29] GONZALEZ-MONTES Y, RODRIGUEZ-ROMANOS R, VILLAVICENCIO A, OSCA-GELIS G, GONZALEZ-BARTULOS M et al. Genetic variants of CTLA4 are associated with clinical outcome of patients with multiple myeloma. Front Immunol 2023; 14: 1158105. https://doi.org/10.3389/fimmu.2023.1158105

[30] NI J, LI C, XU X, XU Q, YIN Q et al. Multi-omics analysis uncovers predictive biomarkers for the efficacy and outcomes of chemoimmunotherapy in advanced unresectable biliary tract cancers. BMC Med 2025; 23: 435. https://doi.org/10.1186/s12916-025-04263-z

[31] ANDRZEJCZAK A, KARABON L. BTLA biology in cancer: from bench discoveries to clinical potentials. Biomark Res 2024; 12: 8. https://doi.org/10.1186/s40364-024-00556-2

[32] MUCCIO VE, SARACI E, GILESTRO M, GATTEI V, ZUCCHETTO A et al. Multiple myeloma: New surface antigens for the characterization of plasma cells in the era of novel agents. Cytometry B Clin Cytom 2016; 90: 81–90. https://doi.org/10.1002/cyto.b.21279

[33] BAE J, ACCARDI F, HIDESHIMA T, TAI YT, PRABHALA R et al. Targeting LAG3/GAL-3 to overcome immunosuppression and enhance antitumor immune responses in multiple myeloma. Leukemia 2022; 36: 138–154. https://doi.org/10.1038/s41375-021-01301-6

[34] NINKOVIC S, PURTON LE, HARRISON SJ, QUACH H. Multiplex immunohistochemistry elucidates increased distance between cytotoxic T cells and plasma cells in relapsed myeloma, and identifies Lag-3 as the most common checkpoint receptor on cytotoxic T cells of myeloma patients. Haematologica 2024; 109: 1487–1500. https://doi.org/10.3324/haematol.2023.283344

[35] CAO LY, ZHAO Y, CHEN Y, MA P, XIE JC et al. CAR-T cell therapy clinical trials: global progress, challenges, and future directions from ClinicalTrials.gov insights. Front Immunol 2025; 16: 1583116. https://doi.org/10.3389/fimmu.2025.1583116

[36] CHEN M, ZHANG B, MU X, ZHANG B, YANG T et al. Recent advances in tumor immunotherapy based on NK cells. Front Immunol 2025; 16: 1595533. https://doi.org/10.3389/fimmu.2025.1595533

[37] DAVAR D, ANDERSON AC, DIAZ-PADILLA I. Therapeutic potential of targeting LAG-3 in cancer. J Immunother Cancer 2025; 13: https://doi.org/10.1136/jitc-2025-011652

[38] KAMALI AN, HAMEDIFAR H, EISENHUT M, BAUTISTA JM. Multiple myeloma and the potential of new checkpoint inhibitors for immunotherapy. Ther Adv Vaccines Immunother 2024; 12: 25151355241288453. https://doi.org/10.1177/25151355241288453

[39] RICHARD S, LESOKHIN AM, PAUL B, KAUFMAN JL, PIANKO M et al. Clinical response and pathway-specific correlates following TIGIT-LAG3 blockade in myeloma: the MyCheckpoint randomized clinical trial. Nat Cancer 2024; 5: 1459–1464. https://doi.org/10.1038/s43018-024-00818-w

[40] GUILLEREY C, NAKAMURA K, PICHLER AC, BARKAUSKAS D, KRUMEICH S et al. Chemotherapy followed by anti-CD137 mAb immunotherapy improves disease control in a mouse myeloma model. JCI Insight 2019; 5: https://doi.org/10.1172/jci.insight.125932

[41] STOLL A, BRUNS H, FUCHS M, VOLKL S, NIMMERJAHN F et al. CD137 (4-1BB) stimulation leads to metabolic and functional reprogramming of human monocytes/macrophages enhancing their tumoricidal activity. Leukemia 2021; 35: 3482–3496. https://doi.org/10.1038/s41375-021-01287-1

[42] DEMPKE WCM, FENCHEL K, UCIECHOWSKI P, DALE SP. Second- and third-generation drugs for immuno-oncology treatment-The more the better? Eur J Cancer 2017; 74: 55–72. https://doi.org/10.1016/j.ejca.2017.01.001

[43] ZHAO X, WANG Y, JIANG X, MO B, WANG C et al. Comprehensive analysis of the role of ICOS (CD278) in pan-cancer prognosis and immunotherapy. BMC Cancer 2023; 23: 194. https://doi.org/10.1186/s12885-023-10564-4

[44] TAN J, JIA Y, ZHOU M, FU C, TUHIN IJ et al. Chimeric antigen receptors containing the OX40 signalling domain enhance the persistence of T cells even under repeated stimulation with multiple myeloma target cells. J Hematol Oncol 2022; 15: 39. https://doi.org/10.1186/s13045-022-01244-0

[45] WANG T, YANG Y, MA L, FENG R, LI J et al. BCMA-BBZ-OX40 CAR-T Therapy Using an Instant Manufacturing Platform in Multiple Myeloma. J Immunother Cancer 2024; 12: https://doi.org/10.1136/jitc-2024-009476

[46] YU T, JIAO JH, WU MF. CAR-T cells in the treatment of multiple myeloma: an encouraging cell therapy. Front Immunol 2025; 16: 1499590. https://doi.org/10.3389/fimmu.2025.1499590

[47] GUILLEREY C, FERRARI DE ANDRADE L, VUCKOVIC S, MILES K, NGIOW SF et al. Immunosurveillance and therapy of multiple myeloma are CD226 dependent. J Clin Invest 2015; 125: 2077–2089. https://doi.org/10.1172/JCI77181

[48] CHU B, BAO L, WANG Y, LU M, SHI L et al. CD27 antigen negative expression indicates poor prognosis in newly diagnosed multiple myeloma. Clin Immunol 2020; 213: 108363. https://doi.org/10.1016/j.clim.2020.108363

[49] SI X, ZHAO J, SONG Y, FU W, ZHANG R. Prognostic value of the expression of CD27 and CD117 in newly diagnosed multiple myeloma patients. BMC Immunol 2025; 26: 40. https://doi.org/10.1186/s12865-025-00719-2

[50] WANG X, LUO K, XU Q, CHI L, GUO Y et al. Prognostic marker CD27 and its micro-environmental in multiple myeloma. BMC Cancer 2024; 24: 352. https://doi.org/10.1186/s12885-024-11945-z

[51] KIM AMJ, NEMETH MR, LIM SO. 4-1BB: A promising target for cancer immunotherapy. Front Oncol 2022; 12: 968360. https://doi.org/10.3389/fonc.2022.968360

[52] CONNER M, HANCE KW, YADAVILLI S, SMOTHERS J, WAIGHT JD. Emergence of the CD226 Axis in Cancer Immunotherapy. Front Immunol 2022; 13: 914406. https://doi.org/10.3389/fimmu.2022.914406

[53] KASAP C, IZGUTDINA A, PATINO-ESCOBAR B, KANG AS, CHILAKAPATI N et al. Targeting high-risk multiple myeloma genotypes with optimized anti-CD70 CAR T cells. Blood 2025; 146: 819–833. https://doi.org/10.1182/blood.2024025536

[54] SHEYKHHASAN M, AHMADIEH-YAZDI A, VICIDOMINI R, POONDLA N, TANZADEHPANAH H et al. CAR T therapies in multiple myeloma: unleashing the future. Cancer Gene Ther 2024; 31: 667–686. https://doi.org/10.1038/s41417-024-00750-2

[55] JAKUBIKOVA J, CHOLUJOVA D, BEKE G, HIDESHIMA T, KLUCAR L et al. Heterogeneity of B cell lymphopoiesis in patients with premalignant and active myeloma. JCI Insight 2023; 8: https://doi.org/10.1172/jci.insight.159924

[56] ZHANG L, PENG X, MA T, LIU J, YI Z et al. Natural killer cells affect the natural course, drug resistance, and prognosis of multiple myeloma. Front Cell Dev Biol 2024; 12: 1359084. https://doi.org/10.3389/fcell.2024.1359084

[57] KUANG Z, LI L, ZHANG P, CHEN B, WU M et al. A novel antibody targeting TIM-3 resulting in receptor internalization for cancer immunotherapy. Antib Ther 2020; 3: 227–236. https://doi.org/10.1093/abt/tbaa022